1-4-2024

On Progress in Exploring Controlled Viscous Limit-Cycle Oscillations in Modified Glauert Airfoil

Ethan Deweese
Embry-Riddle, deweesee@my.erau.edu

Lap Nguyen
Embry-Riddle Aeronautical University, nguye276@erau.edu

Erik Vataker
Embry-Riddle Aeronautical University, vatakere@my.erau.edu

William MacKunis
Embry-Riddle Aeronautical University - Daytona Beach, mackuniw@erau.edu

Vladimir Golubev
Embry-Riddle Aeronautical University, golubd1b@erau.edu

See next page for additional authors

AIAA SciTech Forum
8-12 January 2024, Orlando, FL
AIAA SCITECH 2024 Forum

10.2514/6.2024-1560

On Progress in Exploring Controlled Viscous Limit-Cycle Oscillations in Modified Glauert Airfoil

Ethan Deweese[1], Lap Nguyen[2], Erik Vataker[3], William MacKunis[4], Vladimir Golubev[5],
Embry-Riddle Aeronautical University, Daytona Beach, FL 32114, USA

Ron Efrati[6], Oksana Stalnov[7]
Technion-Israel Institute of Technology, Haifa, Israel

The paper reports on the progress in the development of a novel robust, nonlinear flow control technology that employs an array of synthetic-jet actuators (SJAs) embedded in 2-DOF, elastically mounted, optimized Modified Glauert (MG) airfoil design in order to control limit cycle oscillations (LCO) at low subsonic flow regimes. The focus here is on the conceptual design of the wind energy harvesting system that employs, e.g., a piezoelectric device to extract energy from plunging LCO, with the closed-loop controller being capable to sustain the required LCO amplitudes over a wide range of wind speeds. The current high-fidelity studies first include validation of the static-airfoil aerodynamic predictions against results obtained from the concurrent experimental campaign. Next, a set of parametric 1-DOF and 2-DOF numerical analyses examine open-loop and closed-loop LCO control strategies that employ the ability of MG airfoil to sustain LCO at subcritical velocities due to natural separation-induced flutter.

I. Introduction

Our previous studies [1-2] conducted a benchmark study of the robust flight control approach focusing on the control of the transitional, elastically-mounted, two-degrees-of-freedom (2-DOF) airfoil entering limit-cycle oscillations (LCO) induced by an impinging upstream vortical flow disturbance (e.g., a sharp-edge gust, as illustrated in Fig. 1). The examined methodology combined both low- and high-fidelity analysis tools for design and prediction of synthetic-jet actuator's control authority. A novel robust controller design was proposed in Ref. [1] wherein a rigorous mathematical analysis of the controller performance addressed parametric uncertainties and nonlinearities inherent in the synthetic-jet actuator (SJA) dynamics. The controller design was easily and inexpensively implementable, requiring no observers, function approximators, or adaptive update laws which would be required in alternative methods. Minimal knowledge of the structure of the SJA dynamic model was exploited, with matrix decomposition technique utilized along with innovative algebraic manipulation in the controller development to compensate for the dynamic uncertainty in the SJAs. Results of the low-fidelity reduced-order modeling of LCO robust control demonstrated successful LCO suppression that was achieved for a wide range of the airfoil initial excitation amplitudes with the prescribed set of the controller gains. Subsequently, Ref. [2] focused on extending the low-fidelity study presented in Ref. [1] to include a high-accuracy numerical approach previously employed in our past gust-response [3-4] and SJA-based flow control [5] studies. A representative set of structural parameters from experimental study of Ref. [6] was selected to provide a realistic model of elastically-mounted wing section. The high-accuracy analysis of gust-induced LCO transition was augmented through inclusion of surface-embedded SJAs operating in the closed-loop system, with actuation parameters governed by the robust controller. Using the high-accuracy simulations, the success of the implemented robust control strategy was examined as part of the implicit time-marching numerical procedure.

More recently, a novel nonlinear control algorithm was proposed in Ref. [7] capable of either eliminating or sustaining the optimal amplitude of limit cycle oscillations (LCO) induced on an array of plates, with the latter approach targeting a wind flutter energy extraction system using an optimized Modified Glauert (MG) airfoil design to allow sufficient SJA actuator control authority. The fluid forcing function, which is a function of the fluid flow velocity near the surface of the plate, was designed to control the LCO over a range of wind speeds. In the proposed variable-fidelity, nonlinear closed-loop control approach, a proper orthogonal decomposition (POD)-based model reduction technique is first used to recast the Navier-Stokes equations as a set of nonlinear ordinary differential equations in terms of unknown Galerkin coefficients. The unknown coefficients of the reduced order

[1] Graduate Research Assistant, Department of Aerospace Engineering
[2] Visiting Research Scholar, Department of Aerospace Engineering
[3] Graduate Research Assistant, Department of Aerospace Engineering
[4] Associate Professor, Department of Physical Sciences
[5] Professor, Department of Aerospace Engineering, AIAA Associate Fellow
[6] Graduate Research Assistant, Department of Aerospace Engineering
[7] Assistant Professor, Department of Aerospace Engineering, AIAA Member

model are estimated in finite time using a novel sliding mode estimator. These estimates are used as feedback measurements in a nonlinear control law, with a rigorous proof of finite time estimation for the reduced order model provided in Ref. [7]. In particular, a Lyapunov-based stability analysis was used to prove asymptotic regulation of the flow field velocity to a desired velocity profile, which results in generating the desired fluid forcing function. Preliminary low-fidelity numerical simulation results were obtained to demonstrate the capability of the control system to regulate the fluid forcing function to a desired state, which controls the LCO oscillations.

The current study extends the previous analyses to demonstrate the efficiency of the SJA-based control strategies, particularly in sustaining the plunging LCO in MG airfoil at low subcritical flow velocities. Numerical simulations are first validated against experimental results at static conditions. Next, a set of parametric numerical experiments is conducted to examine the MG airfoil's ability to sustain LCO in both uncontrolled and controlled cases.

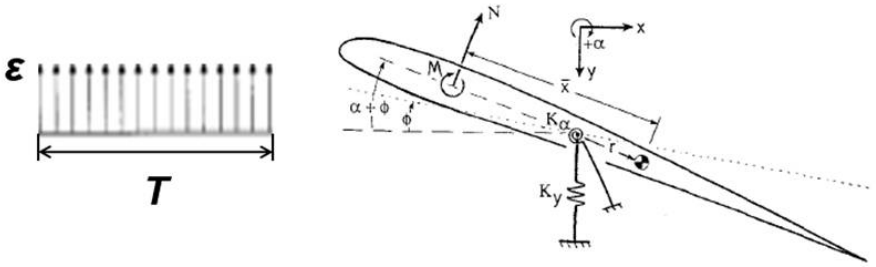

Fig. 1: Model of 2-DOF elastically-mounted airfoil dynamics excited by impinging sharp-edge gust [2].

II. Aeroelastic Response Control Model

In general, the equations describing unsteady response of elastically-mounted 2-DOF airfoil approximated as a flat plate can be expressed as (e.g., Refs. [8-9]),

$$M_s \ddot{p} + C_s \dot{p} + F(p)p = \begin{bmatrix} -Lift \\ Moment \end{bmatrix} \tag{1}$$

where the coefficients $M_s,\ C_s \in \mathbb{R}^{2\times 2}$ denote the structural mass and damping matrices, $F(p) \in \mathbb{R}^{2\times 2}$ is a nonlinear stiffness matrix, and $p(t) \in \mathbb{R}^2$ denotes the state vector. In Eqn. (1), $p(t)$ is explicitly defined as

$$p = \begin{bmatrix} h \\ \alpha \end{bmatrix} \tag{2}$$

where $h(t),\ \alpha(t) \in \mathbb{R}$ denote the plunging [meters] and pitching [radians] displacements describing the LCO effects. Also in Eqn. (1), the structural linear mass matrix M_s is defined as

$$M_s = \begin{bmatrix} m & S_\alpha \\ S_\alpha & I_\alpha \end{bmatrix} \tag{3}$$

where the parameters $S_\alpha,\ I_\alpha \in \mathbb{R}$ are the static moment and moment of inertia, respectively. The structural linear damping matrix is described as

$$C_s = 2\begin{bmatrix} \zeta_h \sqrt{k_h m} & 0 \\ 0 & \zeta_a \sqrt{k_\alpha I_\alpha} \end{bmatrix} \tag{4}$$

where the parameters $\zeta_h,\ \zeta_\alpha \in \mathbb{R}$ are the damping logarithmic decrements for plunging and pitching, and $m \in \mathbb{R}$ is the mass of the wing, or in this case, a flat plate. The nonlinear stiffness matrix utilized in this study is

$$F(p) = \begin{bmatrix} k_h & 0 \\ 0 & k_\alpha + k_{\alpha^3}\alpha^2 \end{bmatrix} \tag{5}$$

where $k_\alpha,\ k_{\alpha^3} \in \mathbb{R}$ denote structural resistances to pitching (linear and nonlinear) and $k_h \in \mathbb{R}$ is the structural resistance to plunging.

In Eq. (1), the total lift and moment are explicitly defined as

$$\begin{bmatrix} -Lift \\ Moment \end{bmatrix} = \begin{bmatrix} -(L + L_{v_j}) \\ (M + M_{v_j}) \end{bmatrix} = M_a \ddot{p} + C_a \dot{p} + K_a p + L_\eta \eta + B\delta \tag{6}$$

where $\delta = \left[-L_{vj}; M_{vj}\right] \in \mathbb{R}^2$ denote the equivalent control force and moment, respectively due to the virtual surface deflection generated by *j*th SJA, and $L,\ M \in \mathbb{R}$ are the aerodynamic lift and moment due to the 2-DOF motions. In Eq. (6), $\eta \in \mathbb{R}^2$ denotes the aerodynamic state vector that relates the moment and lift to the structural modes. Also in Eq. (6), the aerodynamic and mode matrices $M_a,\ C_a,\ K_a,\ L_\eta \in \mathbb{R}^{2\times 2}$ are described as

$$M_a = \pi\rho b^2 \begin{bmatrix} -1 & ba \\ ba & -b^2\left(\frac{1}{8} - a^2\right) \end{bmatrix}, \tag{7}$$

$$C_a = \pi\rho b^2 \begin{bmatrix} 0 & -U \\ 0 & -Ub\left(\frac{1}{2} - a\right) \end{bmatrix} + 2\pi\rho Ub\phi(0) \begin{bmatrix} -1 & -b\left(\frac{1}{2} - a\right) \\ b\left(\frac{1}{2} + a\right) & b^2\left(\frac{1}{2} + a\right)\left(\frac{1}{2} - a\right) \end{bmatrix} \tag{8}$$

$$K_a = 2\pi\rho Ub\phi(0) \begin{bmatrix} 0 & -U \\ 0 & b\left(\frac{1}{2} + a\right)U \end{bmatrix} \tag{9}$$

$$L_\eta = 2\pi\rho Ub \begin{bmatrix} a_1 b_1 & a_2 b_2 \\ -b\left(\frac{1}{2} + a\right)a_1 b_1 & -b\left(\frac{1}{2} + a\right)a_2 b_2 \end{bmatrix} \tag{10}$$

where $\phi(0)$ is the Wagner solution function at 0, and the parameters $a_1,\ b_1,\ a_2,\ b_2 \in \mathbb{R}$ are the Wagner coefficients. The aerodynamic state variables are governed by

$$\dot{\eta} = C_\eta \dot{p} + K_\eta p + S_\eta \eta \tag{11}$$

The aerodynamic state matrices in Eqn. (11), $C_\eta,\ K_\eta,\ S_\eta \in \mathbb{R}^{2\times 2}$, are explicitly defined as

$$C_\eta = \frac{U}{b} \begin{bmatrix} -1 & -b\left(\frac{1}{2} - a\right) \\ -1 & -b\left(\frac{1}{2} - a\right) \end{bmatrix} \tag{12}$$

$$K_\eta = \frac{U}{b} \begin{bmatrix} 0 & -U \\ 0 & -U \end{bmatrix} \tag{13}$$

$$S_\eta = \frac{U}{b} \begin{bmatrix} -b_1 & 0 \\ 0 & -b_2 \end{bmatrix} \tag{14}$$

By substituting Eqn. (6) into Eq. (1) the LCO dynamics can be expressed as

$$M\ddot{p} = -C\dot{p} - Kp + L_\eta \eta + B\delta \tag{15}$$

where $C = C_s - C_a,\ K = F(p) - K_a$ and $M = M_s - M_a$.

The objectives of the current study is to design the control signal $u(t)$ to regulate the plunging and pitching dynamics (i.e., $h(t)$, $\alpha(t)$) to zero or a fixed value. To facilitate the control design, the expression in Eq. (15) is rewritten as

$$M\ddot{p} = g(h, \alpha, \eta) + Bu \tag{16}$$

where $g(h, \alpha, \eta)$ is an unknown, unmeasurable auxiliary function. To quantify the control objective, Ref. [1] introduced a regulation error $e_1(t) \in \mathbb{R}^2$ and auxiliary tracking error variables $e_2(t),\ r(t) \in \mathbb{R}^2$ [7] are defined as

$$e_1 = p - p_d \tag{17}$$

$$e_2 = \dot{e}_1 + \alpha_1 e_1 \tag{18}$$

$$r = \dot{e}_2 + \alpha_2 e_2 \tag{19}$$

where $\alpha_1,\ \alpha_2 > 0 \in \mathbb{R}^+$ are user-defined control gains, and the desired plunging and pitching states $p_d = 0$ for the plunging and pitching suppression objective. Based on the open loop error dynamics, the control input in the original study [1] was designed via

$$\dot{u} = B^{-1}(-(k_s + I_{2\times 2})r - \beta sgn(e_2(t))) \tag{20}$$

where k_s, $\beta \in \mathbb{R}^{2\times 2}$ denote constant, positive definite, diagonal control gain matrices, and $I_{2\times 2}$ denotes a 2×2 identity matrix. Note that the control input $u(t)$ does not depend on the unmeasurable acceleration term $r(t)$, since Eq. (20) can be directly integrated to show that $u(t)$ requires measurements of $e_1(t)$ and $e_2(t)$ only. Using the designed robust control law, Ref. [1] implemented a reduced-order model that showed successful LCO suppression for a selected benchmark case. To this end, the objective of Ref. [2] was to further validate the robust controller model developed based on the 2-DOF inviscid flat-plate dynamics. In particular, a high-fidelity model was developed to study the aeroelastic response and robust LCO control for a realistic 2-DOF viscous airfoil with embedded SJAs. Such model employed in the current study is described in detail below.

III. Fluid Dynamic Model

To demonstrate the developed SJA-based LCO control technology, a high-fidelity numerical approach is examined which employs a modified version of the Implicit Large Eddy Simulation (ILES) Navier-Stokes solver FDL3DI [10]. The following features of the original version of the code are particularly beneficial for the current analysis of fluid-structure interaction and its control:

- Implicit time marching algorithms (up to 4th-order accurate) are particularly suitable for the low-Reynolds number wall-bounded flows characteristic of MAV airfoils.
- High-order spatial accuracy (up to 6th-order accurate) is achieved by use of implicit compact finite-difference schemes, thus making LES resolution attainable with minimum computational expense.
- Robustness is achieved through a low-pass Pade-type non-dispersive spatial filter that regularizes the solution in flow regions where the computational mesh is not sufficient to fully resolve the smallest scales. Note that the governing equations are represented in the original unfiltered form used unchanged in laminar, transitional or fully turbulent regions of the flow. The highly efficient Implicit LES (ILES) procedure employs the high-order filter operator in lieu of the standard SGS and heat flux terms, with the filter selectively damping the evolving poorly-resolved high-frequency content of the solution.
- Overset grid technique is adopted for geometrically complex configurations, with high-order interpolation maintaining spatial accuracy at overlapping mesh interfaces. The code employs an efficient MPI parallelization that has been successfully utilized on various Beowulf cluster platforms in our previous studies.

IV. Numerical Implementation

The current study employs the developed in the code and successfully validated capability to simulate the coupled unsteady aerodynamic and aeroelastic responses of 1-DOF and 2-DOF elastically-mounted airfoils and their transition to LCO induced by an impinging gust (Fig. 1). The aeroelastic response module has been implemented within the framework of the viscous flow solver. In the numerical formulation, the equations governing the fluid dynamics are essentially coupled with equations governing 1-DOF or 2-DOF airfoil motion so that the fluid and structure are treated as a single dynamical system. In the time-marching procedure, the aerodynamic loads are supplied through Navier-Stokes simulations while the structural response module determines the displacement vector which, in turn, defines the grid motion. At each physical time step, the internal iterative loop achieves the balance of the new airfoil position and the corresponding unsteady flowfield. The loop is efficiently merged with the sub-iterative procedure implemented as part of the flow solver's implicit time marching scheme.

A. Impinging Sharp Edge Gust Model

In this study, the airfoil's LCO is induced by an impinging sharp-edge gust, with details of the numerical implementation of the gust-airfoil interaction model presented, e.g., in Ref. [4]. The model is analytically described in terms of the upwash velocity profile (with the streamwise component $u_g(x,t)$=0) in Eq. (21).

$$v_g(x,t) = \begin{cases} \varepsilon_g f(t - x/u_\infty), & u_\infty(t - T_g) \le x \le u_\infty t \\ 0, & otherwise \end{cases} \tag{21}$$

In numerical simulations, such gust is generated with a prescribed duration T_g and the gust amplitude ε_g in the momentum source region located upstream of the airfoil, and undergoes ramp-up and ramp-down phases similar to natural flows as represented by function f in Eq. (21).

B. SJA Model

To simulate active LCO control using synthetic micro-jets, this study adopts the methodology of Ref. [5] where the effectiveness of SJA (Fig. 2) for active control of unsteady flow over SD7003 low-Re airfoil in presence of a sharp-edge gust was investigated. In the adopted numerical procedure, only the actuator's orifice with a properly

defined fluctuating-velocity boundary condition specified by Eqn. (22) is embedded into the airfoil surface to allow for the synthetic jet to freely interact with the grazing boundary-layer flow. In the current simulations, the fluctuating-velocity boundary condition is prescribed directly on the airfoil surface to minimize complexities allowing for a parametric analysis of optimized SJA locations to be performed.

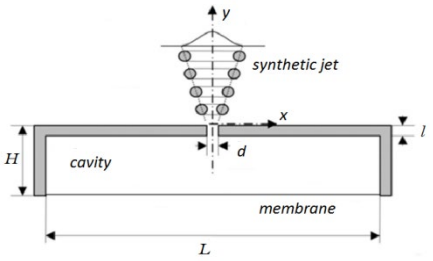

Fig.2: Schematic of synthetic-jet actuator [5].

$$v_{SJA}(x,t) = A\cos(\omega_{SJA}t) \tag{22}$$

C. Modified Glauert Airfoil

The high-accuracy viscous study of Ref. [2] explored SJA-based robust control of gust-induced LCO by first comparing SJA-induced unsteady responses of NACA-0012 airfoil and an airfoil designed by mirroring Glauert airfoil's upper surface profile to the lower surface to obtain a symmetric airfoil referred to in this work as the modified Glauert (MG) airfoil. It was further demonstrated [2] that NACA-0012 airfoil with embedded actuators was not capable to provide sufficient LCO control compared to MG airfoil, and hence all subsequent studies focused solely on MG airfoil analysis. The MG airfoil baseline 1363 × 789 × 3 O-grid is illustrated in Fig. 3. A standard Glauert airfoil is designed to have a large separated region in the aft section of the airfoil [11], which is detrimental to the aerodynamic performance. However, when an SJA is placed and actuated at an optimal location near the separation region, a notable improvement in the aerodynamic response can be achieved. The MG airfoil tested in this work is thus adequate for LCO control based on the improved control authority characteristics.

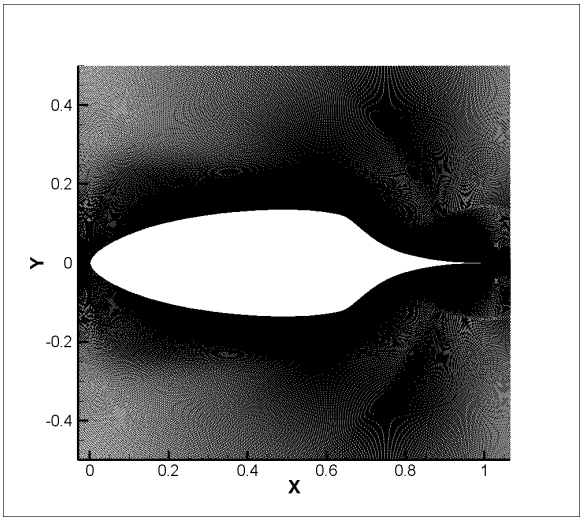

Fig. 3: Numerical grid of MG airfoil.

The boundary conditions imposed consist of a no-slip wall with 4th-order extrapolation at the airfoil surface, periodicity along the span, and a freestream condition imposed at the farfield boundary located more than 100 chords away from the airfoil, with the grid rapidly stretching towards that boundary to ensure effective elimination of spurious reflections achieved in conjunction with the low-pass spatial filtering [10]. A fixed time step of $\Delta t = 9\times10^{-5}$ was used in the code parallel simulations [2], with the baseline mesh efficiently partitioned into a set of 784 overlapped blocks assigned to different processors. Such computations required about 40 CPU hours on a DOD HPC system to establish a clearly-defined LCO in approximately 2×10^{6} time steps.

V. Previous Results

A parametric study was first carried out in Ref. [2] to identify an optimal location for the required control of the flow in the separated regions. This was performed by placing the airfoil at AOA=0 deg and running the simulation

for 20 characteristic cycles at M_∞ =0.056 and *Re*=180,000 to find the separation points. The numerical results predicted the separation point located at approximately 64% chord, similar to the experimental finding of Ref. [11]. It was further revealed that placing the SJA directly at the separation region does not provide the desired results. To this end, the SJA location was varied until the optimal location was found. A thorough parametric investigation revealed that the optimized location existed at around 68% chord for the MG airfoil design. The airfoil thus had two embedded actuators installed at the optimized location, one on top and one on the bottom. Fig. 4 illustrates the comparison obtained for MG airfoil between the cases with no SJA, with non-optimized SJA location, and with the optimized SJA location. The contours show that the optimized SJA location has much weaker vorticity formed in the aft section of the airfoil. When these results are time-averaged as illustrated in Fig. 5, the *U*-velocity contours reveal a much smaller recirculation area in the aft section of the airfoil with a more streamlined flow pattern.

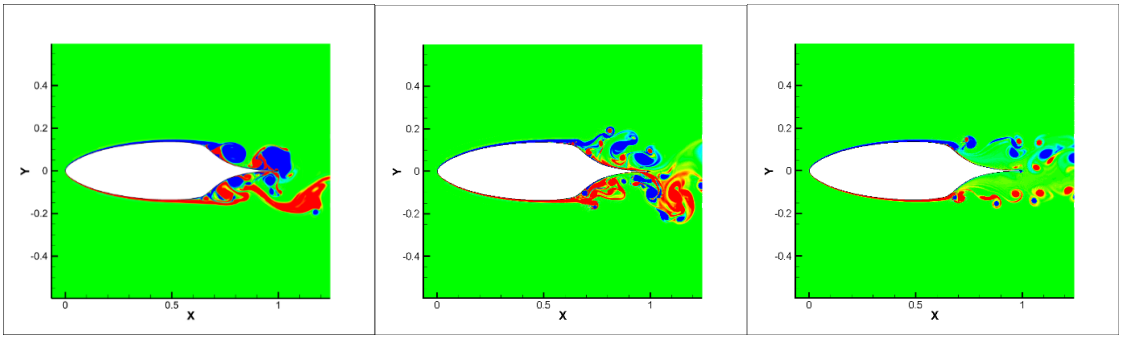

Fig. 4: Z-vorticity contours of no SJA, non-optimized SJA location, and optimized SJA location (left to right).

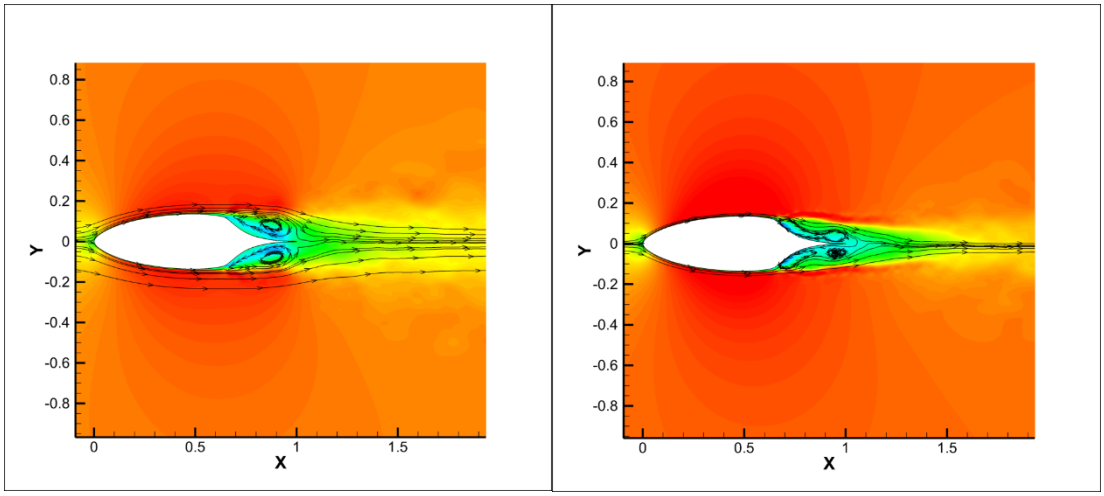

Fig. 5: Time-averaged U-velocity contours of non-optimized SJA location, and optimized SJA location (left to right).

In the current study, a representative set of the aeroelastic model's parameters previously employed in Refs. [1-2] and shown in Table 1 is selected to provide a realistic model of elastically-mounted MG airfoil wing section. These structural parameters match with experimental study in Ref. [6] which indicated a critical (flutter) speed of about 16 m/s in this test case. The robustness of the controller design proposed in Ref. [1] was first validated in a series of simulations where the control gains were kept constant for several different freestream velocities. Fig. 6 shows the suppression of pitching LCO for the upper and lower spectrum of supercritical freesteam velocities 18.25 and 28.5 m/s, respectively. The results show the expected trend of increased time required to suppress LCO at higher flight speeds.

$\rho = 1.1 kg/m^3$	$b = 0.11\, m$	$a = -0.024\, m$
$m = 2.55\, kg$	$a_1 = 0.165$	$a_2 = 0.0455$
$S_\alpha = 1.04\times10^{-2}\, kg\cdot m$	$b_1 = 0.335$	$b_2 = 0.300$
$I_\alpha = 2.51\times10^{-3}\, kg\cdot m$	$k_\alpha = 9.3\, N/m$	$k_{\alpha^3} = 55\, N/m$
$k_h = 450\, N/m$	$\zeta_h = 5.5\times10^{-3}$	$\zeta_\alpha = 1.8\times10^{-2}$

Table 1. Parameters of 2-DOF aeroelastic model [6].

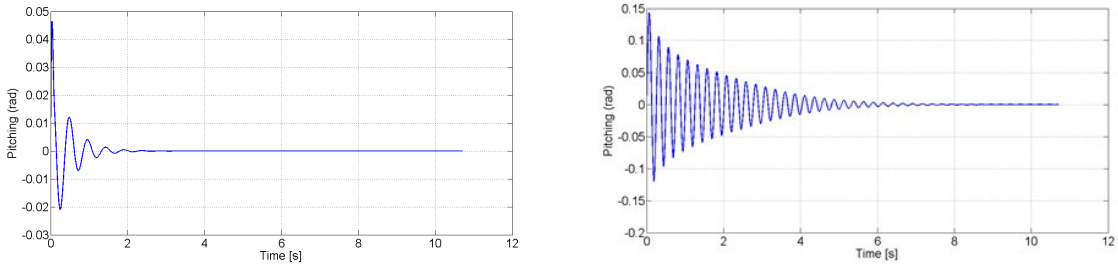

Fig. 6: Suppression of pitching LCO achieved by the feedback-loop robust control system with increasing freestream velocities *(U = 18.25, 28.5 m/s)* based on low-fidelity study [1].

The pitching LCO control was examined as part of the time-accurate viscous simulations conducted for MG airfoil at 19 m/s [2]. For this particular case, a sharp-edge gust shown in Fig. 1 with prescribed duration T_g=5 and gust amplitude ε_g =0.5 was introduced 1.5 chords upstream at T=35 to provide the initial disturbance forcing the airfoil into LCO. The time history of the airfoil pitching response is shown in Fig. 7, with instantaneous z-vorticity contours illustrated in Fig. 8. Clearly, the flow in the aft section of the airfoil is highly separated and benefits from SJAs for reattaching the flow, thus ultimately controlling LCO. It should be noted that for all actuation cases, the amplitude and non-dimensional angular actuation frequency in Eqn. (22) were selected with A=2.0 and ω_{sja} =20, which is 4 times higher than natural shedding frequency $\omega_{shedding}$ =5. The actuation frequency was chosen based on a comparative study in which several actuation frequencies were investigated, ranging from 5-40. The study revealed that between ω_{sja} =5 and ω_{sja} =10, very little change was observed in the aerodynamic response. However, when the actuation frequency was increased to 20, the flow patterns changed and the aerodynamic response showed the actuation to be dominating the flow. The increase from ω_{sja} =20 to ω_{sja} =40 did not show any significant differences.

The SJA-based control simulations were initiated using results from the uncontrolled computations as the input. The difference between the controlled and uncontrolled case is shown in Fig. 7. The pitching motion shows no differences between the two cases initially at T=230, however as the controller begins to drive the SJMAs, the results begin to deviate substantially. The results show the controller to successfully reduce the pitching LCO motion between T=230 and T=300. The reduction in the pitching amplitudes also resulted in a significant drop in moment response.

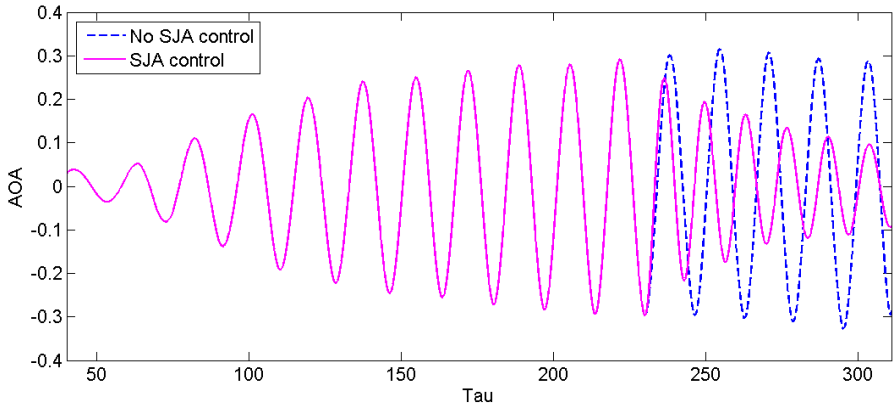

Fig. 7: Time histories of airfoil pitching response for 19m/s with and without SJA LCO suppression [2].

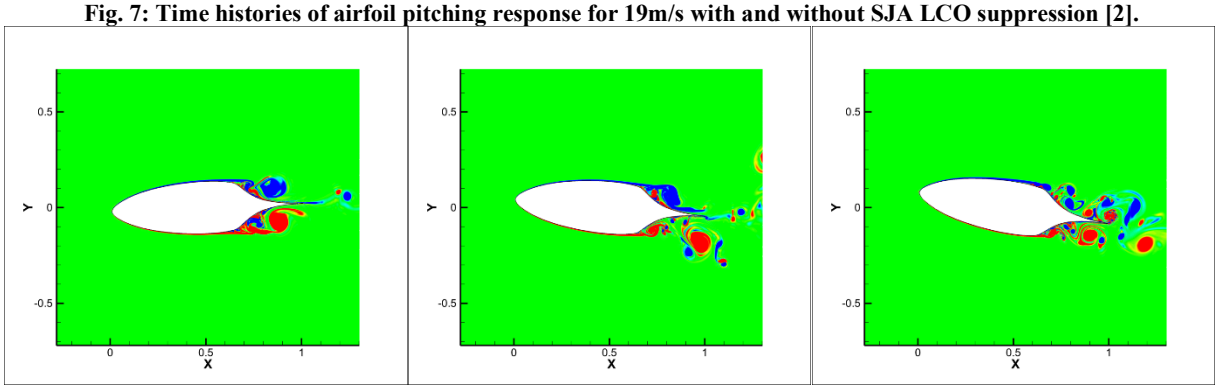

Fig. 8: Z-vorticity contours of suppressed pitching LCO motion at T=226, T=263, and T=303 (left to right) [2].

VI. Current Results and Discussion

Following up on the above-described high-fidelity analysis strategy, the static-airfoil simulations for the flow conditions specified in Table 2 were first conducted and validated against experimental data provided by Technion-Israel Institute of Technology. The case studies were conducted for a range of angles of attack (AOA) 0° to 10° angle of attack in 2° increments, with the resulting pressure distributions presented and compared against XFOIL predictions and experimental data in Figs. 9-11.

$U_\infty = 12$ m/s	Re = 180,000
$\rho_\infty = 1.14$ kg/m^3	$\mu_\infty = 1.841 \times 10^{-5}$ Pa·s
$P_\infty = 98$ kPa	$T_\infty = 299$ K

Table 2. Steady-state flow parameters.

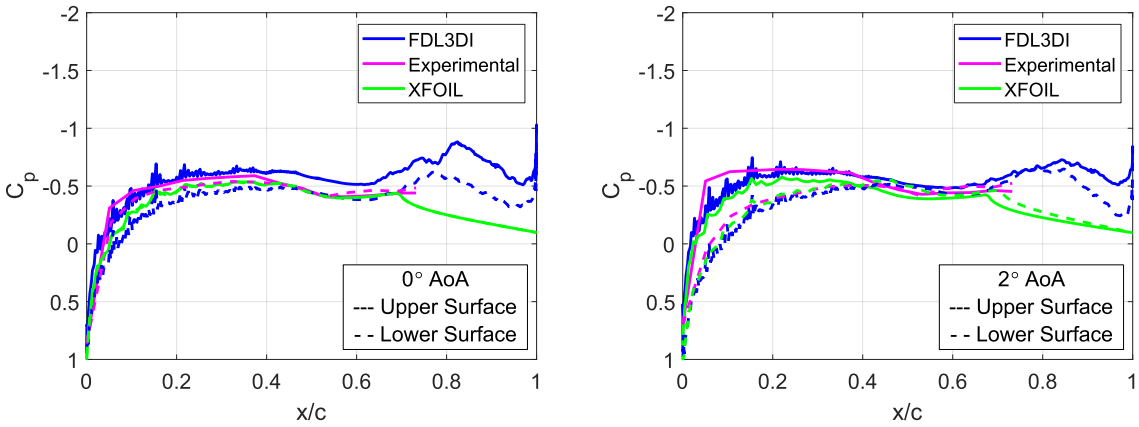

Fig. 9. Pressure coefficient Contours at 0° (left) and 2° (right) angles of attack.

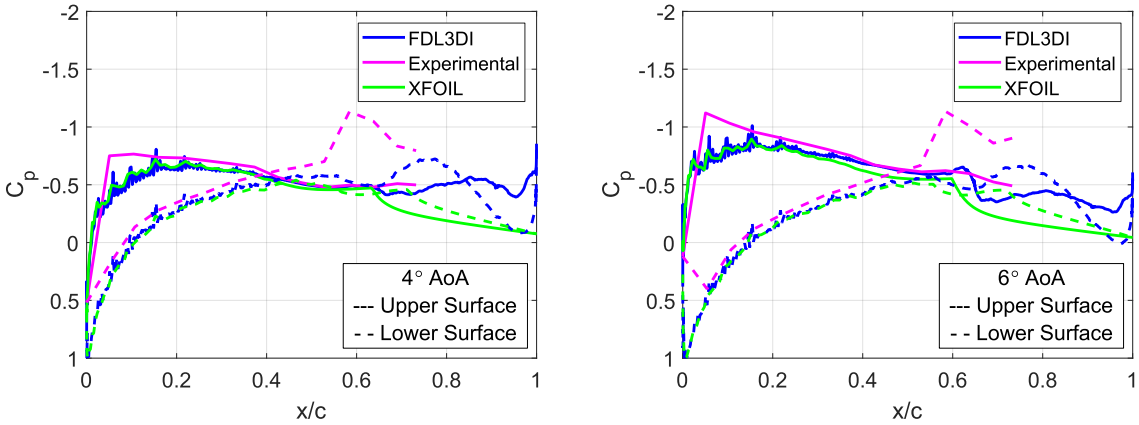

Fig. 10. Pressure coefficient Contours at 4° (left) and 6° (right) angles of attack.

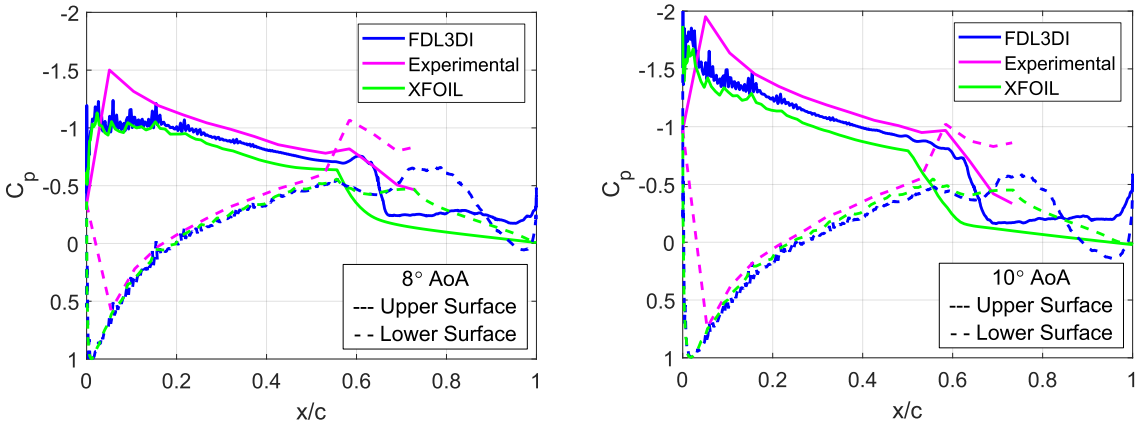

Fig. 11. Pressure coefficient Contours at 8° (left) and 10° (right) angles of attack.

The high-fidelity FDL3DI predictions generally follow the experimental data from the leading edge past the mid-chord of the airfoil where such data is available. The observed noise in the numerical data is a consequence of interpolating the coordinate points defining the airfoil geometry to a much denser numerical grid. Notably, the XFOIL panel-method predictions with viscous correction also compare well with FDL3DI results through the mid-chord region, however generally overpredict the surface pressure in the separated region towards the trailing edge. The latter comparison, in fact, improves at higher angles of attack. The integrated surface pressure data provided with a generally satisfactory lift curve comparison, as shown in Fig. 12. Note that XFOIL code ability to predict well the overall trends in the MG airfoil's aerodynamic response indicates a potential to develop a robust reduced-order airfoil topology optimization tool that could be used in the future optimization studies.

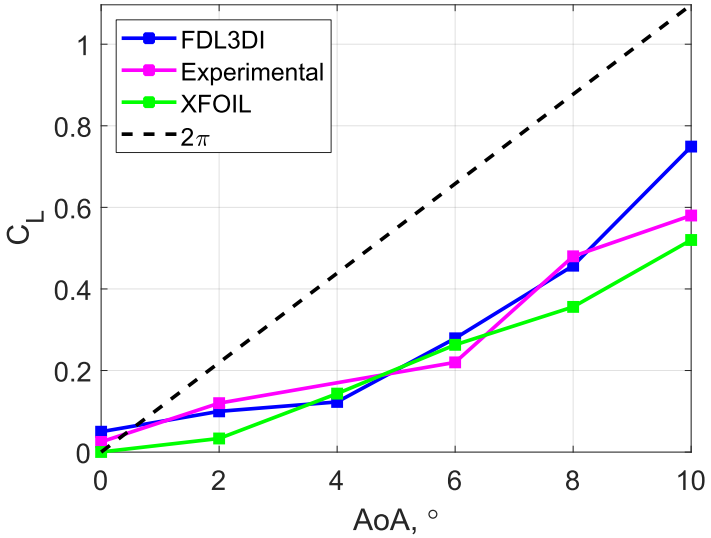

Fig. 12. Lift curve comparison between CFD and experiment.

Extending the previous work evaluating the 1-DOF airfoil pitching response, the current LCO analysis was first conducted to examine the uncontrolled 2-DOF pitching/plunging airfoil dynamics, at the subcritical upstream flow velocity of 7 m/s (Re = 104,200) also considered in all subsequent parametric studies in the current work. Remarkably, the natural laminar separation induced by the MG airfoil shape leads to the sustained LCO despite the free-stream velocity being below the critical flutter speed as predicted by the inviscid theory and confirmed by experimental and numerical data (e.g., [6]). Based on the 2-DOF uncontrolled-case analysis, the time-averaged pitching and plunging frequencies of 4.51 Hz and 1.01 Hz, respectively, were recorded. Further analysis showed that both modes of motion did not reveal a strong coupling, so that the complete removal of the pitching DOF resulted in a similar amplitude and overall behavior of plunging motion, as seen in Fig. 13.

Towards the goal of developing a strategy for SJA-based sustainment and/or amplification of the plunging LCO amplitude, the airfoil static response to SJA actuation was examined. Based on the previous study [2], the synthetic jet operating at 200 Hz with the exit jet velocity amplitude of 13.5 m/s was modeled as a velocity boundary condition applied on both airfoil surfaces at around 67.5% chord position (close to the natural separation point). Following the converged steady state, the airfoil flow was simulated for 4 sec in a static position with the free-stream velocity of 7 m/s without SJA actuation before the upper-surface jet was activated for another 4 sec. The corresponding time-averaged solutions for each flow regime resulted in the pressure and streamline contours compared in Fig. 14. Note that SJA activation reduces the size of the separated region (though not completely reattaching the flow), resulting in a significant increase in pressure on the actuated upper surface, as seen in Fig. 15. This leads to the decreased lift and a positive pitching moment, which thus substantiates the LCO control potential using optimized alternating-surface SJA actuation. The changes in the airfoil aerodynamic response are also evident from the comparison of the lift and moment time histories in Fig. 16.

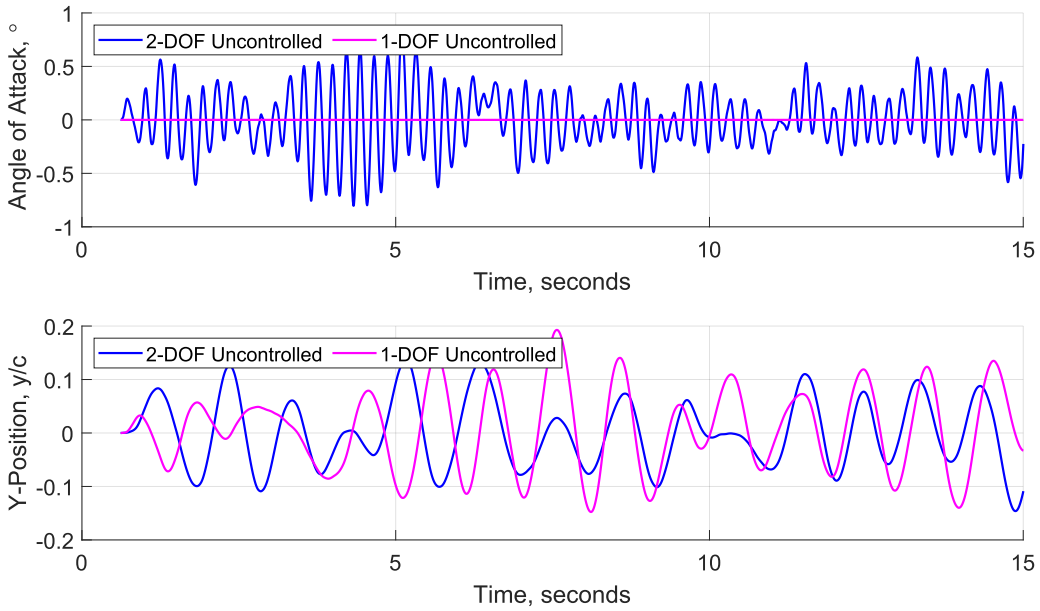

Fig. 13: Time history of pitch and plunge for 2-DOF uncontrolled case at 7 m/s.

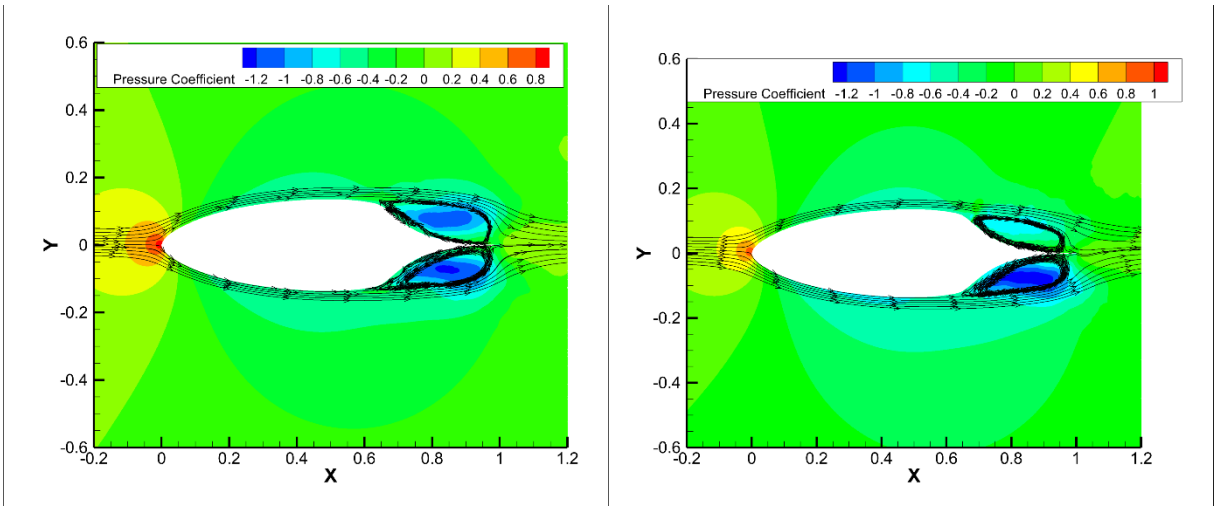

Fig. 14: Comparison of pressure and streamline contours for MG airfoil without SJA actuation (left) and with upper-surface SJA actuation (right).

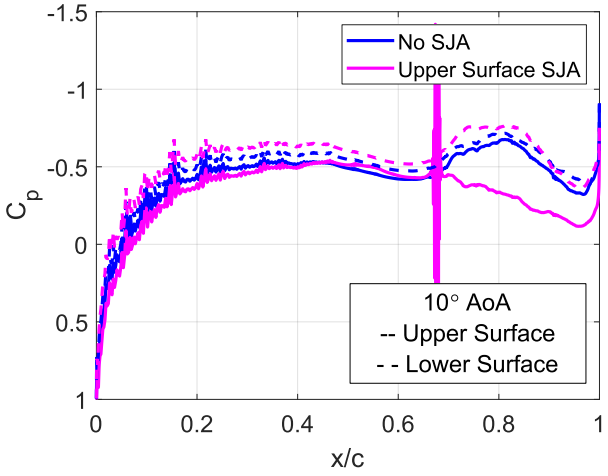

Fig. 15: Comparison of surface pressure distributions with and without SJA actuation.

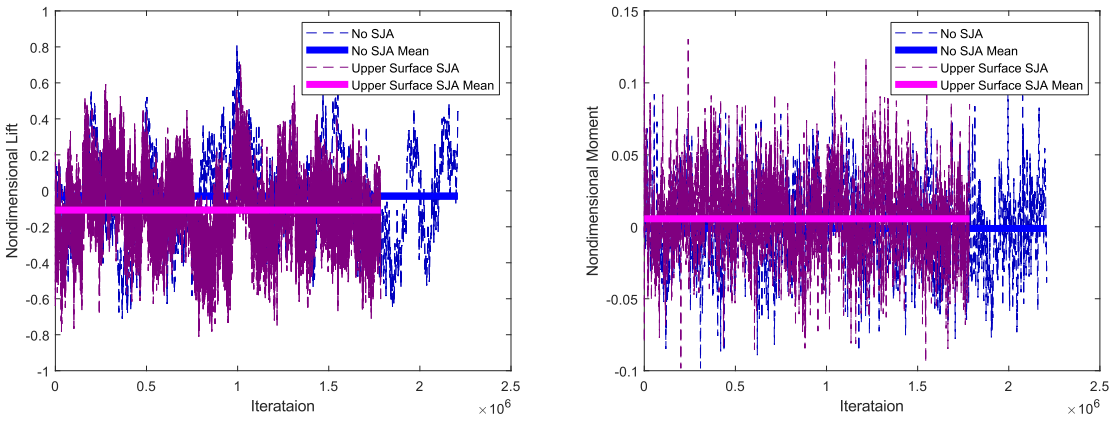

Fig. 16: Time history of lift (left) and moment (right) for the cases with and without SJA actuation.

Both open- and closed-loop modes of SJA-based 2-DOF LCO control are now considered. The open-loop control was first applied by alternating the SJA actuation on the upper and lower airfoil surfaces in sync with the pitching fundamental frequency identified from the uncontrolled case (4.51 Hz), so that each actuation is active for half of one cycle. In contrast, the simplified closed-loop control strategy applied in the current test study to control the pitching LCO "senses" the airfoil angular velocity, and activates the upper-surface SJA when the angular velocity is positive and the lower-surface SJA when it is negative, to ensure the control output is phase-locked to the airfoil motion. The two cases are compared to the uncontrolled case in Fig. 17. Note that both control schemes are able to increase the amplitude of the pitching motion, also resulting in some regularization of the plunging motion (especially in the open-loop case) but without any meaningful increase in the plunging amplitude. To this end, one may conclude that for the current set of structural parameters, the pitching and plunging modes do not reveal a synergetic coupling so that the control schemes implemented with pitching resonant frequency will not be beneficial to the plunging-based wind energy harvesting.

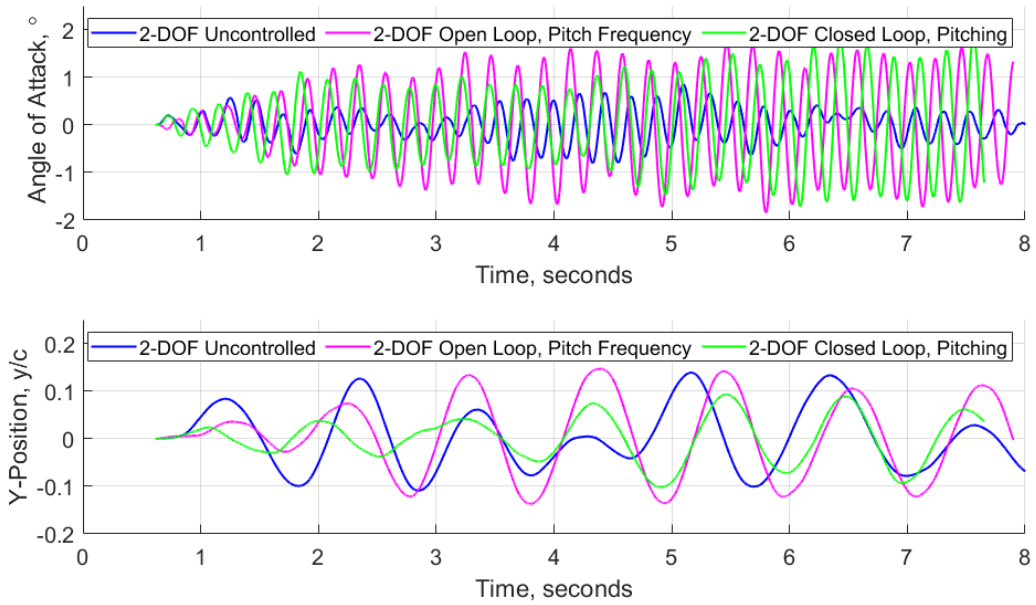

Fig. 17: Time history of pitch and plunge for 2-DOF uncontrolled vs. open- and closed-loop controlled cases, in sync with pitching frequency.

Next, similar open- and closed-loop control schemes are evaluated based on the natural plunging frequency (1.01 Hz) in both 2-DOF and 1-DOF plunging cases. Based on the previous findings, the simplified closed-loop control strategy implements the lower-surface SJA actuation when the positive plunging motion is "sensed". Based on the preliminary test studies, such 1-DOF closed-loop control scheme outperformed the 1-DOF open-loop control strategy for plunging amplitude amplification. With the same objective, 2-DOF open-loop control in sync with the plunging frequency appears to perform slightly better compared to 2-DOF "plunging-focused" closed-loop control strategy described above. Thus, comparing the "winning" strategies with 2-DOF open-loop and 1-DOF closed-loop controls in Fig. 18, both control schemes were successful in roughly doubling the peak amplitude of plunging

(compared to the uncontrolled 1-DOF case) over the observed simulation period. Overall, it may be argued that 1-DOF plunging-only system would be beneficial in its practical implementation (from the standpoint of the system's mechanical design) as the pitching DOF appears redundant and not producing any benefit to the objective of the plunging flutter-based wind energy harvesting.

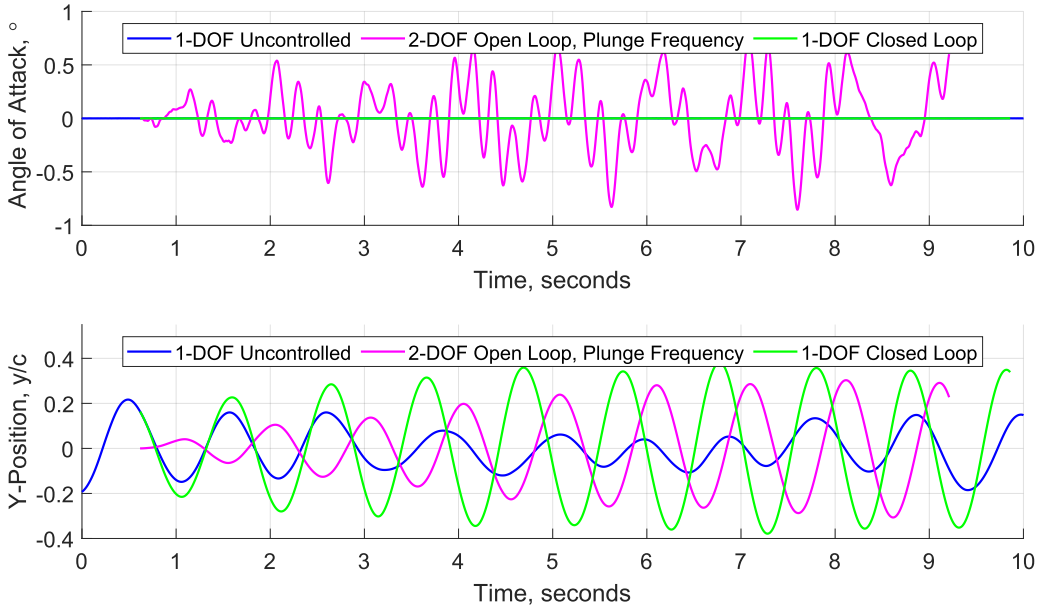

Fig. 18: Time history of pitch and plunge for 1-DOF uncontrolled vs. 2-DOF open-loop and 1-DOF closed-loop controlled cases, in sync with plunging frequency.

VII. Conclusions and Future Work

The current work utilized a high-fidelity analysis to evaluate the uncontrolled vs SJA-based controlled 2-DOF pitching/plunging and 1-DOF plunging LCO observed in MG airfoil at low flow velocities. Even in the uncontrolled cases, the MG airfoil exhibited LCOs at subcritical flow velocities due to its unique shape-induced natural separation phenomenon. The investigated open- and closed-loop SJA-based control schemes were able to further increase the amplitude of the targeted plunging LCO in selected 2-DOF and 1-DOF case studies. On the other hand, 1-DOF plunging-only control would appear beneficial from the standpoint of the mechanical design for the explored flutter-based wind energy harvesting system. The future work will involve the system optimization using a robust reduced-order aerodynamic analysis model such as XFOIL that showed a good comparison with high-fidelity and experimental results in static-airfoil validation studies.

Acknowledgements

The authors would like to acknowledge support for this work from the National Science Foundation (Award Number 1809790). All current simulations were conducted using ERAU's Vega HPC system.

References

1. Ramos Pedroza, N., MacKunis, W., Golubev, V.V., (2017) "A Robust Nonlinear Output Feedback Control Method for Limit Cycle Oscillation Suppression Using Synthetic Jet Actuators," *Aerospace Science and Technology*, Vol. 64, pp. 16-23.
2. Nguyen, L., Golubev, V.V., MacKunis, W., Ramos-Pedroza, N., and Pasiliao, C., (2015), "High-Accuracy Simulations of Robust LCO Control Using Synthetic Jet Actuators," *AIAA Paper 2015-0809*, 53rd AIAA Aerospace Sciences Meeting, Orlando, FL, January 2015.
3. Golubev, V. V., and Visbal, M. R., Modeling MAV Response in Gusty Urban Environment. *International Journal of Micro Air Vehicles*, Vol. 4, (2012), 79–92.
4. L Nguyen, VV Golubev, MR Visbal, (2017) "Numerical Study of Transitional SD7003 Airfoil Interacting with Canonical Upstream Flow Disturbances*," AIAA Journal*, Vol.56, No.1, pp. 158-181.
5. Golubev, V.V., and Nakhla, H., (2012), "Modeling Synthetic Jets for Low-Re Airfoil Unsteady Flow Control," *International Journal of Emerging Multidisciplinary Fluid Sciences*, Vol. 3, 145-158.

6. Berggren, D., (2004) Investigation of Limit Cycle Oscillations for a Wing Section with Nonlinear Stiffness. *Aerospace Science and Technology*. Vol.8, 27-34.
7. W. MacKunis, V. Golubev, K. Kidambi, R Mankbadi, O. Stalnov (2020) "Towards Efficient 2-DOF LCO Control Using a Closed-Loop Nonlinear Active Flow Control Technique", *AIAA Paper 2020-1492*, AIAA SciTech Forum, 6-10 January 2020, Orlando.
8. O'Neil, T.O. and Strganac, T.W., (1998) "Aeroelastic Response of a Rigid Wing Supported by Nonlinear Springs," *Journal of Aircraft*, Vol.35, No.4, 616-622.
9. Bisplinghoff, R.L., Ashley, H. and Halfman, R.L., Aeroelasticity. *Addison-Wesley* (1957).
10. Visbal, M.R., Gaitonde, D.V., (2002) "On the Use of High-Order Finite-Difference Schemes on Curvilinear and Deforming Meshes," *J. Computational Physics*. Vol. 181, 155–185.
11. Yom-Tov, J., Seifert, A., (2005) "Multiple Actuators Flow Control over a Glauert-Goldschmied type Airfoil at Low Reynolds Numbers," *AIAA Paper* 2005-5389.